Int J Thermophys (2018) 39:89
https://doi.org/10.1007/s10765-018-2403-2

ICPPP 18

Thermal Diffusivity of Compounds Loaded with Carbon Nanofibers

C. Vales-Pinzon[1] · D. Gonzalez-Medina[1] · J. Tapia[1] · M. A. Zambrano-Arjona[1] · J. A. Mendez-Gamboa[1] · R. A. Medina-Esquivel[1]

Received: 13 October 2015 / Accepted: 29 May 2018 / Published online: 12 June 2018

Abstract In this work, the thermal enhancement in silicone grease-based compounds as a function of carbon nanofiber (CNF) volume fraction was investigated. The thermal diffusivity of the samples was determined by a photopyroelectrical technique with a sample thickness scan. The results show that heat transport on these compounds strongly depends on the CNF volume fraction, due to the high thermal conductivity of CNF compared to the matrix; hence, a low loading percentage of the fibers produce a significant growth in the thermal diffusivity of the composite. The results show that the thermal diffusivity values of the CNF-silicone composite are comparable with commercial thermal compounds based on diamond and Ag microparticle fillers. The thermal conductivity of the samples was calculated, and its enhancement was analyzed using a modified Lewis–Nielsen model, taking into account the dependence of the maximum packing fraction and the form factor with the aspect ratio of the CNF. The influence of the Kapitza thermal resistance was discussed. These materials might find practical applications in systems in which the CNF improves the ebbing of heat away from semiconductor devices or in any other application in which heat dissipation is needed.

Keywords Carbon nanofiber · Thermal compound · Thermal diffusivity

This article is part of the selected papers presented at the 18th International Conference on Photoacoustic and Photothermal Phenomena.

✉ R. A. Medina-Esquivel
ruben.medina@correo.uady.mx; rmedina.esquivel@gmail.com

[1] Facultad de Ingeniería de la Universidad Autónoma de Yucatán, Av. Industrias no Contaminantes por Periférico Norte, Apdo. Postal 150 Cordemex, Mérida, Yucatán, México

1 Introduction

High-power electronics, high-performance heat sinks, aerospace and aircraft industry, systems for storage and generation of energy are some examples of technological applications that require the precise control of heat dissipation [1, 2]. There is a growing demand for the development of new composites with controlled thermal properties. Thermal pastes are commonly based on polymers such as sodium silicate or silicone [3]. To enhance its thermal qualities, the polymer matrix is filled with thermally conductive solid particles like silver, diamond, and alumina, among others [4].

Carbon nanofibers (CNF) are novel nanometric materials with an extensive use in science and engineering because of their exceptional thermal and mechanical physical characteristics [5, 6]. This carbon allotrope represents the base of novel nanometric materials, promising in most areas of science and engineering [5, 7]. It has been shown that when the nanofibers are incorporated into a matrix, the physical properties of the compound are superior to those of the matrix. The thermal properties of carbon nanostructures, such as CNF, are of interest for basic scientific knowledge as well as for technological applications [8–10].

In this work, the thermal behavior improvement of silicone-based compound due to the effect of CNFs loads is analyzed. The thermal characterization of the silicone compounds was performed by means of the photopyroelectric methodology, where a thickness fluid scan is performed through a cylindrical cavity in which CNF compound is placed and measured by height variation. This methodology has become a regular photothermal methodology to obtain the thermal diffusivity of fluids (gases, liquids, and soft matter), as a consequence of its accuracy, precision, and practicality [11–16]. The thermal diffusivity of the studied materials was determined, and the results were compared with other commercial thermal conductive compounds loaded with microparticles of silver and diamond.

2 Experimental

2.1 Materials

Three kinds of thermal compounds were studied, two commercial and one developed in the laboratory using fully graphitized carbon nanofibers with 150 nm average diameter and 50 μm to 200 μm in length (PR-19-XT-HHT, Pyrograf®-III) mixed with a fluid matrix of silicone grease (sil-glyde from AGS). Using a one-step mix process, samples with CNFs were dispersed by sonication at 20 kHz for a period of 2 min with a titanium probe immerse in the grease matrix controlled with an ultrasonic processor. Composites samples with CNFs at different volume concentrations: 0 %, 0.1 %, 0.25 %, 0.5 %, 1 %, 2 %, and 5 % were obtained. The commercial thermal compounds used to compare are: Arctic Silver 5® that consists of a mixture of polysynthetic oils loaded with silver microparticles [17] and IC Diamond®, a thermal compound based on diamond microparticles [18].

2.2 Experimental Technique

The scheme of the experimental system used in the measurement of the thermal diffusivity of the samples is shown in Fig. 1. Basically, the measurement device consists of a cylindrical cavity where the fluid sample is located (see Fig. 1B). The top surface of the thermal wave cavity is a 500-μm-thick crystalline silicon slice that acts as an optically opaque and thermally thin material (Fig. 1B, c). It is excited by a modulated light source from a laser diode (Fig. 1B, a) (ML120G21, 80 mW@658 nm). The beam radiation intensity was modulated (frequency $f = 0.5$ Hz) using a laser diode driver (Thorlabs, IP500) controlled by a lock-in amplifier internal sine oscillator (Stanford Research, SR-830). The laser radiation hits the silicon slice by its outer thermal wave cavity side; thus, the silicon wafer absorbs some of the energy and a heat flow is produced; hence, the wafer merely performs as the converter of the laser energy into heating. The modulated power source generates a periodic flow of heat within the material to generate a periodic temperature distribution at the same frequency as the heating laser; thereby the heat wave propagates in the cavity through the fluid sample (Fig. 1B, d) [19, 20]. The sample thickness is in the thermally thick regime, which causes an exponential decay in the signal; this is then detected at the other end of the cavity by a circular PZT ceramic working as a pyroelectric sensor (Fig. 1B, e). The AC voltage signal is proportional to the surface temperature detector; duly, the pyroelectric sensor measures the time-dependent temperature variation. The output voltage signal-to-noise ratio of the pyroelectric sensor was greatly enhanced by a voltage preamplifier (Stanford Research, model SR-560), and then with a dual phase DSP lock-in amplifier, the phase, and amplitude of the sensor complex voltage are evaluated as a function of the cavity length, which is controlled by a translation stage (with a minimum size step of 10 μm) automated with a mechanically coupled stepper motor. The cavity length scans were performed for sample thickness that satisfies the condition $L > 2\sqrt{\frac{\alpha}{\pi f}}$ (thermally thick regime), where L is thermal cavity length. The acquisition of the amplitude and phase of the sensor voltage and the cavity length scanning were performed by a LabView home-made program.

In the Thermal Wave Resonator Cavity, and for thermally thick samples measured by transmission, the complex voltage of the pyroelectric sensor comes by the following equation

$$V(L, \alpha, f) = F(f) \exp\left[-L(i+1)\sqrt{\pi f/\alpha}\right] \tag{1}$$

where α is the thermal diffusivity and L is the thickness of the fluid sample, $F(f)$ is a transfer function that depends on the modulation frequency of the heating laser. For a fixed heating laser frequency f and sample thickness scanning, this instrumental transfer function may not be taken into account in the measurement and calculation of the thermal diffusivity. The amplitude and phase of Eq. 1 are analyzed separately, and from both parameters, it is possible to get the thermal diffusivity (α) of the CNF-silicone compounds. From the amplitude, we get that $\ln|V| = c_V - \sqrt{\frac{\pi f}{\alpha}}L$, which indicates that the logarithm of the voltage amplitude behaves linearly with respect to the fluid sample thickness L, where the thermal diffusivity α is directly extracted from

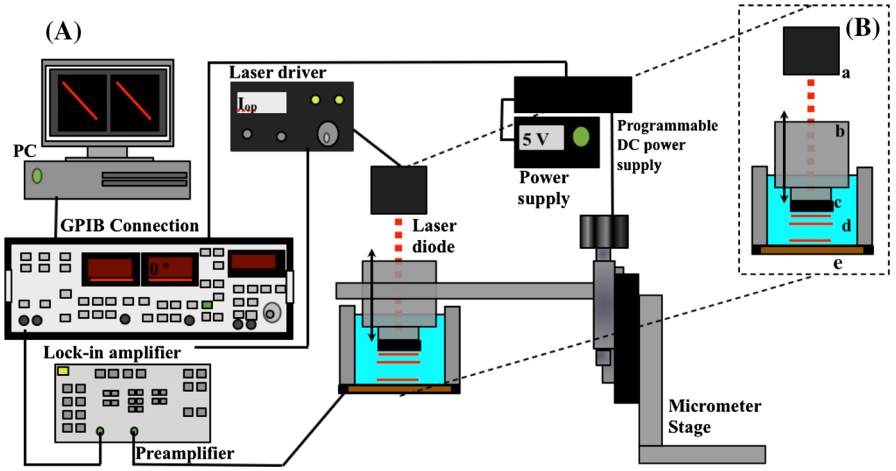

Fig. 1 (A) Experimental arrangement scheme of the pyroelectric technique, to acquire the thermal diffusivity of the silicone CNF compounds. (B) Pyroelectric technique configuration details: (a) laser diode, (b) cylindrical thermal wave emitter head containing the silicon wafer (c), (d) sample container and (e) pyroelectric sensor

the slope of the line. Similarly, from the analysis of the phase, it could be seen that it follows a linear behavior, written as $\Phi = c_\Phi - \sqrt{\frac{\pi f}{\alpha}}L$. It is evident that constants c_V and c_Φ are not important in the calculus of the sample thermal diffusivity.

The linear behavior of the natural logarithm of the amplitude and phase depending on the thickness could be observed in Fig. 2. Therefore, by means of a thickness scan of the fluid sample under a heating with a constant frequency, and defining the slopes as $m_V = m_\Phi = \sqrt{\frac{\pi f}{\alpha}}$, the thermal diffusivity of the sample is determined by the next expressions, for both, the signal amplitude and its phase,

$$\alpha = \frac{\pi f}{m_V^2} \quad \text{or} \quad \alpha = \frac{\pi f}{m_\Phi^2} \tag{2}$$

The thermal diffusivity values found from the signal phase and its amplitude have small variations between them, five measurements were done for every sample with different CNF volume fraction, and two values obtained from each; one for the phase and the other from the amplitude. The final effective thermal diffusivity was the average of these ten values for each concentration; the error bars come from the standard deviation of the mean thermal diffusivity value.

3 Results

Figure 2 shows the linear behavior of the phase and amplitude logarithm of the pyroelectric sensor voltage, in relation to the thickness of the fluid sample. The lines with lower slopes indicate that a slight signal diminishing and phase shift are presented, which means that thermal diffusivity is higher for samples loaded with a low fraction

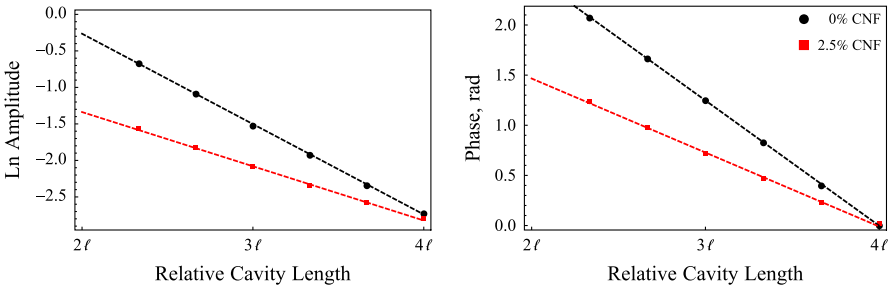

Fig. 2 Linear behavior of the phase and amplitude logarithm of the pyroelectric sensor voltage, related to the thickness of the fluid sample. The parameter ℓ is the thermal diffusion length, defined as $\ell = \sqrt{\alpha/\pi f}$

of CNF than silicone grease without nanostructures. It is relevant to mention that the thermal diffusivity could be obtained from the signal amplitude and signal phase, and the data are consistent between them.

The thermal diffusivity of thermally conductive compounds made from the mixing of graphitized CNF and silicone grease as a function of the CNF volume fraction is presented in Fig. 3. Thermal diffusivity increases with the volume fraction of CNF, as could be expected due to the high thermal conductivity of CNF with respect to the silicone matrix and also due to its high aspect ratio. In Fig. 4, a comparison between the thermal diffusivity as a function of mass fraction of the commercial thermally conductive compounds and the one we developed with CNF is shown, where Arctic Silver 5® has 88 % silver microparticles concentration [15], with a measured $6.40 \pm 0.17 \times 10^{-3}$ cm^2·s^{-1} effective thermal diffusivity, and IC Diamond® containing diamond microparticles concentration of 92 % [16], with a thermal diffusivity value of $4.16 \pm 0.07 \times 10^{-2}$ cm^2·s^{-1}. It is possible to observe a very similar thermal diffusivity value among them, despite the fact that there is a difference of almost one order of magnitude in the mass fraction of loads, between the commercial pastes and the one prepared with the CNF on silicone grease at its maximum fiber load. Specifically, the thermal diffusivity of the CNF-silicone compounds exceeded the value measured for the Arctic Silver 5 paste, and the data behavior of the prepared sample suggest that for higher CNF concentrations, equivalent to IC Diamond sample mass fraction, the thermal diffusivity could reach higher values. Unfortunately, it was not possible to obtain reliable measurements for samples with CNF volume fractions above 0.05, due to a significant viscosity increase and hence a lack of fluency in the compound. Fluidity in the sample is essential for the good performance of the pyroelectric technique used in this work, where the thickness sample scans must be implemented.

In classical effective models, the increase in conductivity and thermal diffusivity, as a function of filler concentration behaves linearly in the case of low concentrations [21]. However, Fig. 3 shows a singular increase in thermal diffusivity as the mass fraction of CNF increases. Currently, there are several theoretical models that predict the effective thermal conductivity of composite materials; the simplest and most usual models generally consider the volume fraction of the filler and the thermal conductivity of the components. However, more complex theoretical models such as the one proposed by Lewis and Nielsen [22], take into account the orientation, shape and

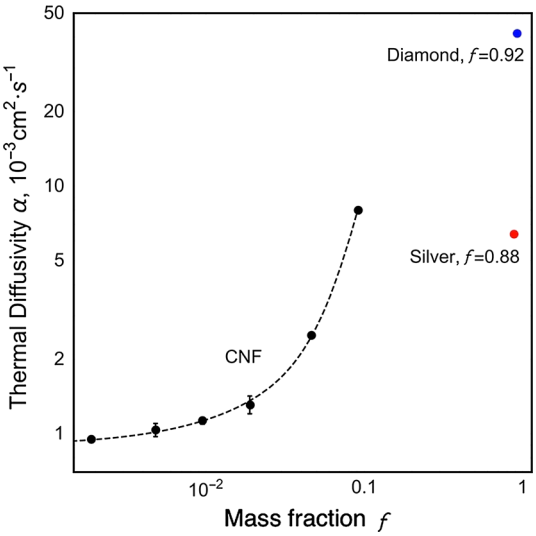

Fig. 3 Thermal diffusivity as a function of mass fraction of the commercial thermally conductive compounds and samples of silicone grease loaded with CNF. The dashed line is a visual aid that denotes the tendency of the experimental values

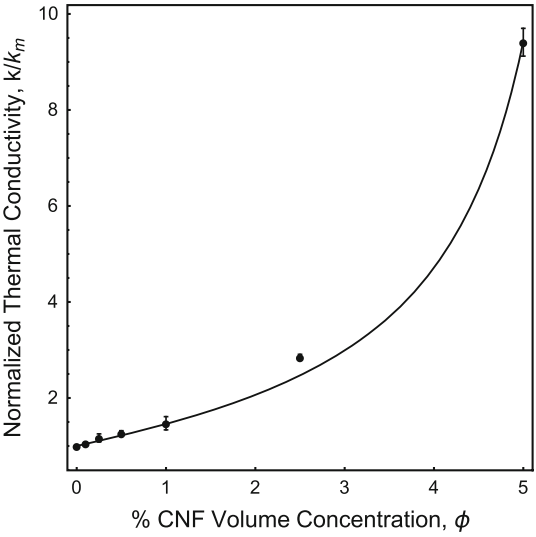

Fig. 4 Normalized thermal conductivity of samples as a function of filler volume fraction. The line is for the theoretical fitting using Eq. 6 for the modified Lewis–Nielsen model

maximum packing fraction ($\phi_{\max}$) of fillers. Particularly for this work, where long filler particles (CNFs) have 10^4 times higher thermal conductivity than the silicone matrix, the effective thermal conductivity of the composite should have a significant growth when filler concentration achieves values near $\phi_{\max}$, since the average number of contacts that each particle has with its neighbors (defined as the coordination number $\langle C \rangle$), significantly increased [23, 24]. Those links work as pathways for thermal or electrical transport through the particles that shape a network; to take thermal advantage of this tridimensional grid, the particles must have a high aspect ratio, high thermal conductivity and a low interfacial thermal resistance between them and

between the matrix. The thermal resistance between interfaces is known as the Kapitza thermal resistance (R_K) [25]; this parameter is essential in the thermal transport of compounds with nanoscale fillers since the thermal resistance is inversely proportional to filler size, which is the radius in the case of nanotubes and nanofibers. An intuitive manner to see the importance of the interface resistance is through the concept of Kapitza radius, defined as $A_k = \frac{k_m}{G}$, where k_m is the matrix thermal conductivity (0.17 $W{\cdot}m^{-1}{\cdot}K^{-1}$, for the silicone used in this work), and G is the conductance of the interface $\left(G = \frac{1}{R_K}\right)$, thus, if the Kapitza radius is near the nanotube or nanofiber radius, the interfacial resistance will negatively influence the effective thermal conductivity of the composite. According to literature [26], the thermal conductance of a liquid–solid interface in the case of carbon nanotubes is $G = 12\ MW{\cdot}m^{-2}{\cdot}K^{-1}$. In the case of the present work, due to carbon nanofibers are graphitized, it is reasonable to consider that liquid–solid conductance of CNFs is the same as the one of carbon nanotubes, the Kapitza radius for this interface conductance is $A_k = 14$ nm. As the carbon nanofibers radius used in this work is $a = 75$ nm, the normalized Kapitza thermal resistance $\alpha_k = \frac{A_k}{a}$ is $\alpha_k = 0.19$, this means that the interfacial thermal resistance does not significantly affect the effective thermal conductivity of the CNF-silicone composite. Such is the contrary case of carbon nanotube fillers with radius around 14 nm, which is the reason that although nanotubes form a connected tridimensional grid, the composite effective thermal conductivity will remain low because the Kapitza thermal resistance predominantly determines the conductivity.

Once the negative influence of the thermal interface resistance is discarded, the analysis of the thermal conductivity behavior is accomplished by taking into account the essential parameters of the composite filler, which are the particle shape, the aspect ratio, and the maximum packing fraction. From the last parameter, $\phi_{max} = \frac{\langle C\rangle D}{2L}$, where D and L are the diameter and length of the filler particles respectively, Wouterse et al. [24] showed that for high aspect ratio (λ) particles, the coordination number value is $\langle C\rangle = 10$. For the high aspect ratio CNFs used in this work (Pyrograph PR-19-XT-HHT, $D = 150$ nm, and L is between 50 and 200 μm), the maximum packing fraction is given by $\phi_{max} = 10\frac{D}{2L} = \frac{5}{\lambda}$; therefore, the theoretical maximum packing fraction is between 1.5 % and 3.8 %. The experimental data are analyzed using the Lewis–Nielsen model, given by

$$\frac{k}{k_m} = \frac{1 + AB\phi_F}{1 - B\psi\phi_F} \tag{3}$$

$$B = \frac{\frac{k_F}{k_m} - 1}{\frac{k_F}{k_m} + A} \tag{4}$$

$$\psi = 1 + \left(\frac{1 - \phi_{max}}{\phi_{max}^2}\right)\phi_F \tag{5}$$

where k is the thermal conductivity of the sample, k_F and k_m are the thermal conductivities of the filler and matrix, respectively. This ratio is known as normalized thermal conductivity. ϕ_F is the volume fraction of the filler and its form factor A depends on the shape, particle orientation and aspect ratio of the dispersed fibers. The form factor

for randomly oriented fibers is related to their aspect ratio λ in such a way that for fibers with $\lambda = 2$, $A = 1.58$; $\lambda = 4$, $A = 2.08$; $\lambda = 6$, $A = 2.8$; $\lambda = 10$, $A = 4.93$ and for $\lambda = 15$, $A = 8.38$ [22]. It can be inferred that A for randomly oriented fibers is a function of the λ and could be simplified as $A = \frac{\lambda}{2}$. Similarly, according to Ref. [24], the maximum volumetric fraction can be written as $\phi_{\max} = \frac{10}{2\lambda} = \frac{5}{\lambda}$. Then, equation [3–5] could be written as a function of λ in the next form:

$$\frac{k}{k_{\mathrm{m}}} = \frac{1 + \lambda B \phi_{\mathrm{F}}/2}{1 - B\psi\phi_{\mathrm{F}}} \tag{6}$$

$$B = \frac{\frac{k_{\mathrm{F}}}{k_{\mathrm{m}}} - 1}{\frac{k_{\mathrm{F}}}{k_{\mathrm{m}}} + \lambda/2} \tag{7}$$

$$\psi = 1 + \lambda \left(\frac{\lambda - 5}{25} \right) \phi_{\mathrm{F}} \tag{8}$$

Instead of the thermal diffusivity being related to CNF mass fraction, the composite thermal conductivity as a function of volume fraction is needed to make use of the modified Lewis–Nielsen model, the thermal conductivity was calculated with the thermal diffusivity values through the equation $k = \alpha\rho C_{\mathrm{p}}$. The volume fraction ϕ_{F} was determined using the densities of CNF, silicone grease and CNFs mass fraction f. Figure 4 shows the normalized thermal conductivity and the fitting through the modified Lewis–Nielsen model, the CNFs aspect ratio that produces the best fitting within the experimental values, is $\lambda = 81.9$, hence $\phi_{\max} = 0.061$.

The range of the CNF aspect ratio from the diameter and length given by the producer (Pyrograph, Inc.) is $\lambda = [333, 1333]$, with this aspect ratio values, the theoretical $\phi_{\max}$ of the CNFs is in the range $\phi_{\max} = [0.015, 0.038]$. Clearly, the aspect ratio and maximum packing fraction of the CNF from the datasheet given by the producer are highly different from the calculated using the Lewis–Nielsen model for the thermal conductivity of the studied CNFs composites. The reduction in λ and therefore the increasing in $\phi_{\max}$ could be a consequence of the CNF sonication mixing process into the silicone matrix, as is reported in literature [27]

The feasibility to get a compound based on particles with high electrical and thermal conductivity in relation to the matrix, allows that final compound has an increase in these properties by increasing its volumetric fraction. However, a very different behavior has been found between the electrical and thermal conductivity as a function of the concentration for compounds [28]; in fact, many investigations related to the study of thermal conductivity in this type of systems denote the absence of a behavior related to percolation. However, in this work, it is possible to see a remarkable increase in the diffusivity and thermal conductivity, which can be explained due to the wide difference between the thermal conductivity of the CNF and the matrix, along with an experimental volumetric concentration close to the maximum packing fraction predicted by the Lewis–Nielsen model, in which it would have the formation of a continuous network of nanostructures coupled with a lack of an important thermal interface resistance for the used CNFs.

4 Conclusions

The photopyroelectric technique used in this work is an effective method to measure the thermal diffusivity of thermally conductive fluid compounds. The results confirm that CNFs even at a low concentration of 5 % in volume (around 9 % in mass) induces a remarkable enhancement (near an order of magnitude) of the effective thermal diffusivity of the conductive compound in comparison with the commercial compounds that mostly used spherical-like particles. Furthermore, the thermal diffusivity of the samples of silicone grease loaded with CNFs could be compared to the thermal diffusivity of the commercial thermally conductive compounds loaded with a much higher silver particles concentration and also with the advantage of a very appreciable lower viscosity. The thermal conductivity of the CNF, its high aspect ratio, and low interface thermal resistance are conditions that enable the substantial enhancement in the effective thermal conductivity of this kind of composites.

Acknowledgments This work was supported by SEP-CONACYT-CB-135131, SEP-CONACYT-CB-182982, SEP-CONACYT-CB-256497.

References

1. A.A. Koga, E.C.C. Lopes, H.F.C. Nova, C.R. de Lima, E.C.N. Silva, Int. J. Heat Mass Transf. **64**, 759–772 (2013)
2. D.D.L. Chung, Carbon **50**, 3342–3353 (2012)
3. Y. Xu, X. Luo, D.D.L. Chung, J. Electron. Packag. **124**, 188–191 (2002)
4. C. Lin, D.D.L. Chung, J. Mater. Sci. **42**, 9245–9255 (2007)
5. S. Zhiqiang, L. Jingfeng, L. Qing, N. Tongyang, W. Gang, Carbon **50**, 5605–5617 (2012)
6. C. Vales-Pinzon, G. Quiñones-Weiss, J.J. Alvarado-Gil, R. Medina-Esquivel, Int. J. Thermophys. **36**, 2854–2861 (2015)
7. S.G. Prolongo, M.R. Gude, A. Ureña, J. Nanosci. Nanotechnol. **9**, 61811–61817 (2009)
8. R.A. Bulante. U.S. Patent 5949650, September (1998)
9. C. Chiu, J.C. Shipley, C.B. Simmons. U.S. Patent 6651736 (2003)
10. V. Gandikota, G.F. Jones, A.S. Fleischer, Exp. Therm. Fluid Sci. **34**, 554–561 (2010)
11. A. Mandelis, J. Vanniasinkam, S. Budhudu, A. Othonos, M. Kokta, Phys. Rev. B **48**, 6808–6821 (1993)
12. J. Shen, A. Mandelis, B.D. Aloysius, Int. J. Thermophys. **17**, 1241–1254 (1996)
13. J. Shen, A. Mandelis, T. Ashe, Int. J. Thermophys. **19**, 579–593 (1998)
14. J. Shen, A. Mandelis, Rev. Sci. Instrum. **66**, 4999–5005 (1995)
15. J.A. Balderas-Lopez, A. Mandelis, J.A. Garcia, Rev. Sci. Instrum. **71**, 2933 (2000)
16. R.A. Medina-Esquivel, C. Vales-Pinzon, G. Quinones-Weiss, M.A. Zambrano-Arjona, J. Mendez-Gamboa, J.J. Alvarado-Gil, Diam. Relat. Mater. **53**, 45–51 (2015)
17. http://www.arcticsilver.com/as5.htm
18. http://innovationcooling.com/index.html
19. R.A. Medina-Esquivel, J.M. Yáñez-Limón, J.J. Alvarado-Gil, Eur Phys J Spec Top **153**, 75–77 (2008)
20. D. Dadarlat, C. Neamtu, R. Pop, M. Marinelli, F. Mercuri, J. Optoelectron. Adv. Mater **9**, 2847–2852 (2007)
21. C.W. Nan, R. Birringer, D.R. Clarke, H. Gleiter, J. Appl. Phys. **81**, 6692–6699 (1997)
22. L.E. Nielsen, Ind. Eng. Chem. Fundam. **13**, 17–20 (1974)
23. W. Evans, R. Prasher, J. Fish, P. Meakin, P. Phelan, P. Keblinski, Int. J. Heat Mass Transf. **51**, 1431–1438 (2008)
24. A. Wouterse, S. Luding, A.P. Philipse, Granul Matter **11**, 169–177 (2009)
25. P.L. Kapitza, in *Collected Papers*, vol. II, ed. by P.L. Kapitza, D. ter Haar (Pergamon Press, Oxford, 1967)

26. S.T. Huxtable, D.G. Cahill, S. Shenogin, L. Xue, R. Ozisik, P. Barone, M. Usrey, M.S. Strano, G. Siddons, M. Shim, P. Keblinski, Nat. Mater. **2**, 731–734 (2003)
27. P. Vichchulada, M.A. Cauble, E.A. Abdi, E.I. Obi, Q. Zhang, M.D. Lay, J. Phys. Chem. C **114**, 12490–12495 (2010)
28. G. Zhang, Y. Xia, H. Wang, Y. Tao, G. Tao, S. Tu, H. Wu, J. Compos. Mater. **44**, 963–970 (2010)